© 2022. Published by The Company of Biologists Ltd | Development (2022) 149, dev200112. doi:10.1242/dev.200112

RESEARCH REPORT

Elevated numbers of infiltrating eosinophils accelerate the progression of Duchenne muscular dystrophy pathology in *mdx* mice

Marine Theret*, Lucas Rempel, Joshua Hashimoto, Morten Ritso, Lin Wei Tung, Fang Fang Li, Melina Messing, Michael Hughes, Kelly McNagny and Fabio Rossi

ABSTRACT

Eosinophils, best known for their role in anti-parasitic responses, have recently been shown to actively participate in tissue homeostasis and repair. Their regulation must be tightly controlled, as their absence or hyperplasia is associated with chronic disease (e.g. asthma or inflammatory bowel disease). In the context of skeletal muscle, eosinophils play a supportive role after acute damage. Indeed, their depletion leads to strong defects in skeletal muscle regeneration and, in the absence of eosinophil-secreted interleukin (IL) 4 and IL13, fibro-adipogenic progenitors fail to support muscle stem cell proliferation. However, the role of eosinophils in muscular dystrophy remains elusive. Although it has been shown that eosinophils are present in higher numbers in muscles from *mdx* mice (a mouse model for Duchenne muscular dystrophy), their depletion does not affect muscle histopathology at an early age. Here, we evaluated the impact of hyper-eosinophilia on the development of fibrofatty infiltration in aged *mdx* mice and found that muscle eosinophilia leads to defects in muscle homeostasis, regeneration and repair, and eventually hastens death.

KEY WORDS: Inflammation, Eosinophil, Regeneration, Repair, Fibrosis, Muscular dystrophy, Mouse

INTRODUCTION

Eosinophils are key effector cells of the type 2 inflammatory response (Th2). Their development and activation are due to the production of IL5, IL3 and GM-CSF by type 2 innate lymphoid cells (ILC2) and CD4+ helper T cells (Dougan et al., 2019). Dysregulation of the Th2 response often results in blood and tissue eosinophilia, mediating chronic diseases such as asthma or inflammatory bowel disease (Bochner et al., 2012; Rodrigo-Muñoz et al., 2021). For example, in the intestine, eosinophils participate in the deposition of a fibrotic scar after irradiation (Takemura et al., 2018). In addition, aging has been associated with increased circulating eosinophils and their primary chemotaxin: CCL11 (eotaxin-1) (Brigger et al., 2020).

In healthy individuals, skeletal muscle regeneration is a multi-step process in which multiple cell types interact in a coordinated fashion (Oprescu et al., 2020). Fibrosis, in contrast, is a hallmark of severely impaired muscle repair, as seen in the incurable chronic disease Duchenne muscular dystrophy (DMD). DMD is an X-linked genetic disease affecting 1 in 3500 boys (Bladen et al., 2015) in which the *DMD* gene contains mutations that result in a lack of dystrophin protein, or in the production of a non-functional truncated form, leading to degeneration followed by chronic cycles of inflammation-regeneration (Dadgar et al., 2014). More recently, the lack of dystrophin in satellite cells (SC) has been shown to impair their behavior and contributes to the pathogenesis of DMD (Dumont et al., 2015). Degeneration is associated with the activation and differentiation of tissue-resident fibro-adipogenic progenitors (FAP) that drive matrix production and the formation of a fibrotic scar, as well as adipocyte differentiation and lipid deposition (Joe et al., 2010; Uezumi et al., 2010, 2011). Likewise, recruited inflammatory macrophages play an important role in the establishment of the fibrotic scar (Lemos et al., 2015; Juban et al., 2018; Chazaud, 2020; Juban, 2021). Intriguingly, an increase in eosinophil infiltration was reported in *mdx* mice, as well as in DMD patients compared with healthy adults (Cai et al., 2000; Kastenschmidt et al., 2021). This has been associated with the development of fibrosis in muscle, which is promoted by the release of major basic protein (MBP) and likely other toxic granule proteins (Cai et al., 2000; Wehling-Henricks, 2004; Wehling-Henricks et al., 2008; Schröder et al., 2013). Currently, corticosteroid treatment is the only effective clinical intervention to delay DMD progression and Prednisone, a well-known corticosteroid, drastically reduces the number of eosinophils present in muscle (Cai et al., 2000; Wehling-Henricks, 2004). On the other hand, eosinophil infiltration in myositis – a term that describes a number of muscle inflammatory diseases of diverse etiology – is not always associated with poor outcomes or with more severe pathology (Selva-O'Callaghan et al., 2014).

The regenerative capacity of skeletal muscle rests on SCs, also called muscle stem cells (MuSC), or muscle progenitors (MP) during regeneration (Lepper et al., 2011; Murphy et al., 2011; Sambasivan et al., 2011). After damage, MuSCs activate, proliferate and initiate the myogenic program to differentiate into myoblasts, which either fuse with existing myofibers or with each other to form new myofibers. A subset of MuSCs will self-renew and return to quiescence in order to maintain the pool of stem cells for further needs (Sacco et al., 2008; Giordani et al., 2018). Concomitantly, inflammatory cells (leukocytes and granulocytes) infiltrate the tissue and direct MP and FAP behavior by secreting various cytokines such as IL1β and TNFα (Arnold et al., 2007; Saclier et al., 2013; Otis et al., 2014). Infiltrating monocytes differentiate into Ly6C+ inflammatory macrophages, stimulating MP proliferation and inducing FAP death. Inflammatory macrophages then lose the expression of Ly6C as they skew to a pro-regenerative phenotype,

School of Biomedical Engineering, Department of Medical Genetics, University of British Columbia, 2222 Health Sciences Mall, Vancouver, BC V6T 1Z3, Canada.

*Author for correspondence (mtheret@brc.ubc.ca)

M.T., 0000-0002-8059-8756; L.R., 0000-0002-8876-3496

Handling Editor: Paul Martin
Received 17 August 2021; Accepted 16 February 2022

Development (2022) 149, dev200112. doi:10.1242/dev.200112

stimulating MP differentiation, myofibre growth and FAP survival via the production of TGFβ, IL6 and NAMPT, among other factors (Arnold et al., 2007; Saclier et al., 2013; Varga et al., 2016; Ratnayake et al., 2021). Although this skewing process is well characterized in acute injury, recent studies suggest a misregulation of macrophage inflammatory function in *mdx* mice (Juban et al., 2018).

In acute injury, eosinophils are essential for efficient skeletal muscle regeneration, as ΔdblGATA mice, which lack eosinophils, display delayed regeneration (Heredia et al., 2013). Indeed, eosinophils participate in muscle regeneration via IL4/IL13 secretion, resulting in the activation of the trophic functions of FAPs towards MPs. Interestingly, although muscle eosinophilia has been described in *mdx* muscle, their depletion by crossing the *mdx* mice with a second strain of eosinophil-deficient mice (PHIL strain) did not improve the histopathology at an early age (Sek et al., 2019). Moreover, the authors also reported no changes in the histopathology of young *mdx* mice that overexpress IL5 (and display blood eosinophilia) (Sek et al., 2019). Importantly, this study only focused on *mdx* mice from 3 to 5 weeks of age, a very narrow period which corresponds to the acute inflammatory onset of the disease rather than its fibrotic progression (Pastoret and Sebille, 1995; Tidball et al., 1995; Muller et al., 2001). Thus, the long-term effect of hyper-eosinophilic infiltration on muscle regeneration, repair and fibrosis remains to be investigated. Based on these observations, we sought to confirm the potential toxic role of eosinophils in muscle using Tg(Cd3d-Il5)NJ.1638Nal mice (hereafter designated IL5-Tg; Lee et al., 1997). Here, we demonstrate that hyper-eosinophilia has an adverse effect on muscle repair, resulting in strong collagen deposition and eventually death.

RESULTS AND DISCUSSION

Muscle eosinophilia impairs skeletal muscle regeneration

As reported previously (Lee et al., 1997), IL5-Tg mice exhibit severe blood eosinophilia [>50% circulating white cells compared with <3% in wild-type (WT) mice, Fig. S1A,B]. To evaluate the effects of hyper-eosinophilia on muscle repair, notexin (NTX) was injected in the tibialis anterior (TA) muscle to elicit acute skeletal muscle injury, and muscle regeneration was analyzed histologically at 7, 14, and 28 days post damage (Fig. 1A-C). Quantification of the number of nuclei per fiber, as well as myofiber cross-sectional area (CSA) showed a significant delay in skeletal muscle regeneration as reflected first by a reduction in the number of nuclei per fiber at 7 days post damage (−13%; P=0.054; Fig. 1B). Furthermore, the size of newly formed myofibers was reduced at 14 and 28 days post damage (−17%, P=0.076; and −23%, P<0.001) (Fig. 1C). Interestingly, it has been reported that eosinophils stimulate tissue-resident FAPs, which, in return, enhance MP proliferation (Heredia et al., 2013). After confirming muscle eosinophilia (Fig. S1C,D), we analyzed FAP and MP proliferation by 5-ethynyl-2′-deoxyuridine (EdU) incorporation (Fig. S1E). Although we noticed an increase in EdU incorporation 1 day post injury, suggesting that MPs exit quiescence faster (+273.6%, P=0.058; Fig. S1F,G), MP proliferation was not affected at 3 and 5 days post injury (Fig. 1D,E) suggesting that MPs undergo an immediate exit of quiescence post injury. No change in FAP proliferation was detected in the IL5-Tg mouse model (Fig. 1F,G). Lastly, eosinophils have been described as a specific source of TGFβ and IL4, which could skew macrophages from a pro-inflammatory (Ly6C+) to a pro-regenerative (Ly6C−) phenotype. In our system, however, the proportion between these two subsets was not affected (Fig. 1H), but we did notice a decrease in the total number of macrophages (Fig. S1H) and especially a reduction in the total number of Ly6C− macrophages per muscle (Fig. 1I,J). Overall, these results suggest that hyper-eosinophilia affects MP early activation and macrophage infiltration, delaying MP fusion and myofiber growth.

Hyper-eosinophilia does not affect FAP trophic function toward myogenic cells

As eosinophils have been described to stimulate FAP trophic function toward MPs (Heredia et al., 2013), we decided to co-culture single WT myofibers with activated FAPs from WT or IL5-Tg muscles. SC proliferation (EdU/MyoD) and differentiation (myogenin) were analyzed at 48 h and 72 h (Brun et al., 2018; Fig. S2A,D). As previously shown (Fiore et al., 2016), WT FAPs strongly enhance SC proliferation compared with the no FAP control condition (CT), shown by an increase in EdU+ cells at 48 h (P<0.05; Fig. S2B) and by an increase in the number of cells per clone at 72 h (P<0.05; Fig. S2E). Furthermore, by analyzing the different states of SC activation (Fig. S2C), we observed that co-cultivating myofibers with FAPs alters the proportional commitment as shown by the decreased percentage of MyoD+ cells (P<0.05 and P<0.01) and increased percentage of proliferating Pax7/EdU/MyoD+ cells (P<0.05 and P<0.01). Interestingly, the only difference noted between WT and IL5-Tg co-culture was an increase in MyoD/EdU+ cells, which is consistent with the slight increase in activation observed *in vivo* (Fig. S1F). However, this early difference did not result in defects in SC proliferation (Pax7+/EdU+), differentiation (myogenin+) or return to quiescence (measured indirectly by Pax7+/EdU−/myogenin− cells) at 72 h (Fig. S2D-F). These results demonstrate that the effect seen previously is likely due to the hyper-eosinophilia, and not to a defect in FAP trophic functions.

Hyper-eosinophilia is not a marker for Th2 inflammation

Although eosinophils are typically described as Th2 inflammatory cells, such as in adipose tissue (Rothenberg and Hogan, 2006; Rana et al., 2019), it is now accepted that they can also acquire different inflammatory profiles depending on their stimulation, and especially a Th1-antiviral-response (Drake et al., 2016). The authors demonstrated that, similar to macrophages, eosinophils from IL5-Tg mice were able to show a Th1 signature after treatment with *E. coli*, IFNγ or a combination of the two (Dolitzky et al., 2021). Interestingly, as skeletal muscle regeneration relies on both Th1 (IFNγ) and Th2 (IL4) responses (Arnold et al., 2007; Heredia et al., 2013), it is not surprising that eosinophils would display both Th1 and Th2 markers. To explore this possibility, WT and IL5-Tg eosinophils were sorted at 3 days post damage and subjected to RNA-sequencing (RNA-seq). Principal component analysis (PCA) indicated a clear transcriptomic difference between WT and IL5-Tg eosinophils (Fig. 2A). Compared with the WT samples, 1155 differentially expressed genes (DEGs) were discovered (676 upregulated and 479 downregulated DEGs; Table S3). By focusing on known cytokines and chemokines produced by eosinophils (Rothenberg and Hogan, 2006; Dolitzky et al., 2021), we were able to show that many of the upregulated DEGs in IL5-Tg eosinophils included both Th1 and Th2 markers such as *Cd36*, *Cd274*, *Car4*, *Lair1*, *Cd101*, *Tgfb1* and *Vegfa* (Fig. 2B). Interestingly TGFβ1 has been recently shown to negatively impact MP fusion. Thus, an increase in this factor could explain the delay in skeletal muscle regeneration, and specifically the decrease in number of nuclei per fiber (Fig. 1B) (Girardi et al., 2021). Moreover, it is important to note the upregulation of *Epx* and *Prg2* (MBP), which are enzymes known to contribute to the pathology of the DMD (Cai et al., 2000;

Development (2022) 149, dev200112. doi:10.1242/dev.200112

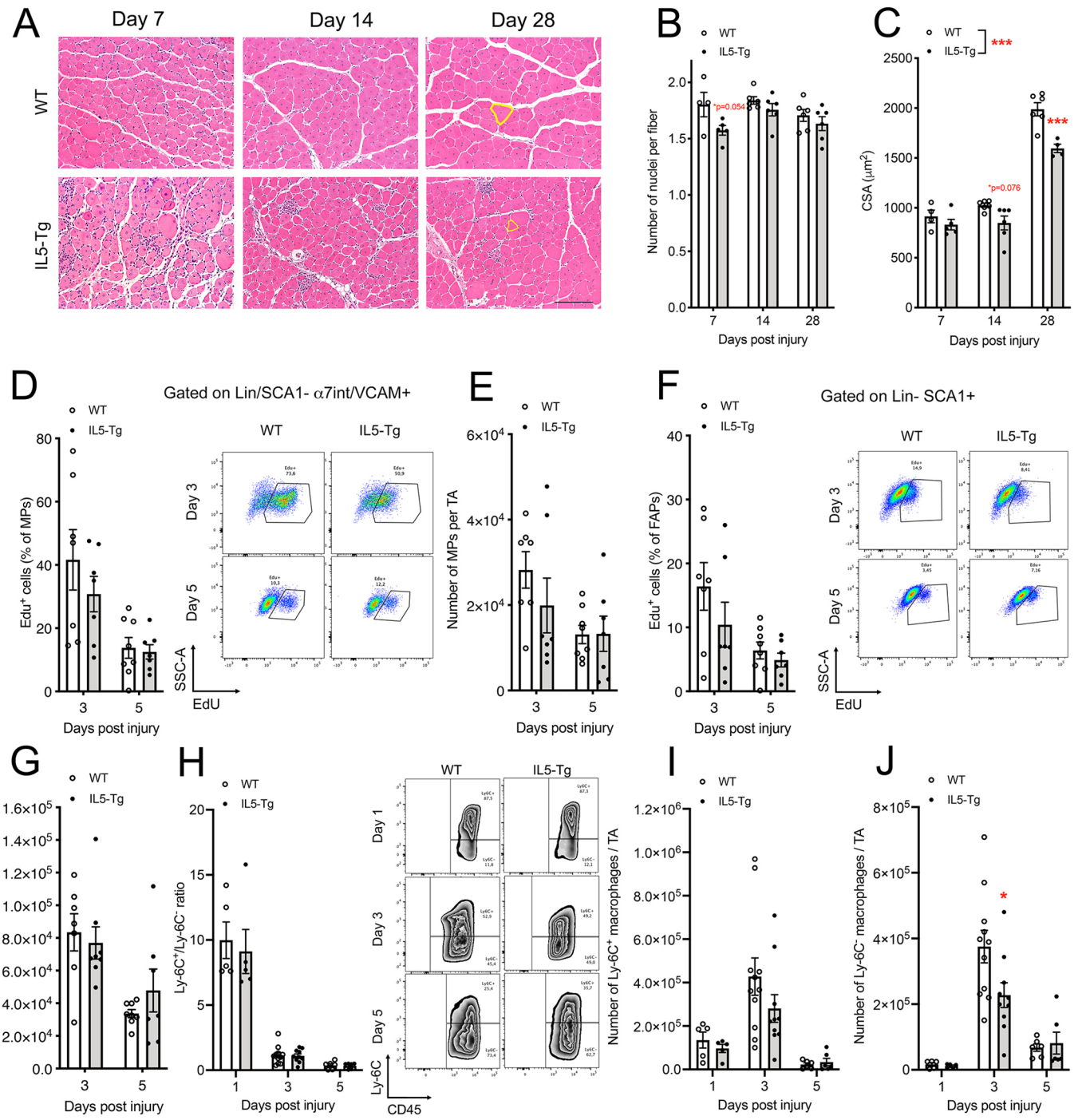

Fig. 1. Skeletal muscle regeneration is delayed in IL5-Tg mice. (A-C) Tibialis anterior (TA) muscles were damaged with notexin (NTX) and harvested at 7, 14 and 28 days post injury. (A) TAs were sectioned and stained with H&E. Yellow line indicates cross-sectional area measurement. (B,C) Quantification of number of nuclei per fiber (B) and myofiber cross-sectional area (CSA) (C). *n*=4-6. (D-G) Quantification by flow cytometry of 3 and 5 days post-NTX injury assessment of myogenic progenitor (MP; D,E) and fibro-adipogenic progenitor (FAP; F,G) proliferation, measured by EdU incorporation (D,F) and their total number per TA (E, G). *n*=7-8. (H-J) Macrophage polarization was followed at 1, 3 and 5 days post injury by the quantification of the expression of Ly6C using flow cytometry (H). The total number of Ly6C+ (I) and Ly6C− (J) macrophages was also quantified. *n*=5-11. Wild type (WT) versus IL5-Tg: **P*<0.05, ****P*<0.001 [two-way ANOVA was performed followed by post-hoc testing (Šidak multiple comparison)]. Gaussian distribution was not assumed. Data are mean±s.e.m. Scale bar: 100 µm.

Wehling-Henricks et al., 2008). Lastly, IL5-Tg eosinophils express less *Il4*, which could explain the observed decrease in macrophage numbers and, in particular, the pro-regenerative Ly6C− macrophages (Fig. S1H-J). It is important to note that macrophage skewing was not studied in the ΔdblGATA mice, as the authors state that both inflammatory and pro-regenerative macrophages infiltrate the tissue after damage (Heredia et al., 2013). However, the authors do not report defects in skeletal muscle regeneration in mice lacking the IL4R in myeloid cells (LysM^{CRE}:IL4R^{flox} mice), suggesting that IL4 is either not crucial for macrophage polarization, or that compensatory mechanisms exist in this model (Heredia et al., 2013). Overall, our observations are discordant with the paradigm that eosinophils (and

Development (2022) 149, dev200112. doi:10.1242/dev.200112

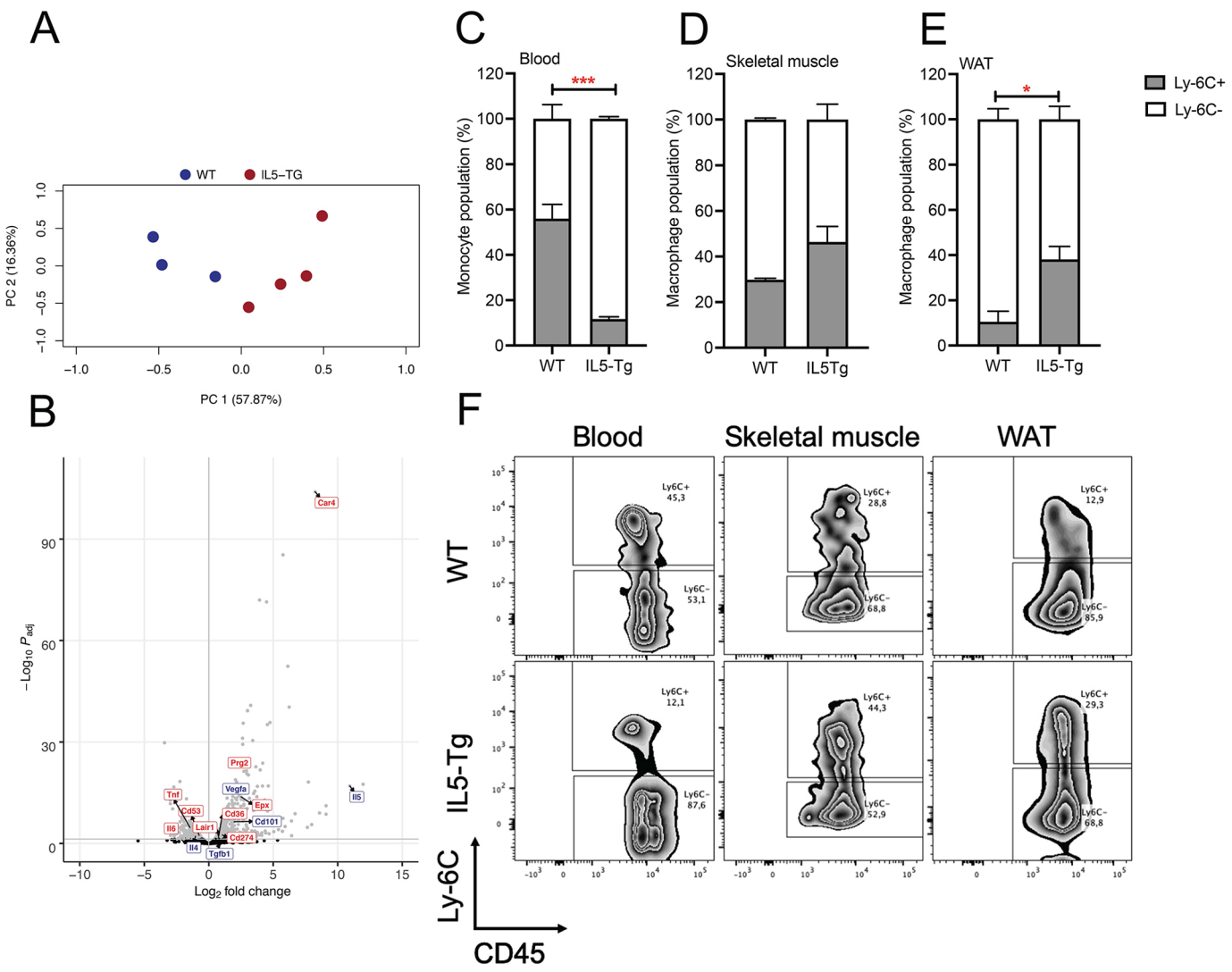

Fig. 2. The IL5-Tg eosinophil inflammatory profile does not correspond to Th2 inflammatory response. Eosinophils from wild-type (WT) and IL5-Tg mice were sorted from damaged muscles at 3 days post-injury. (A,B) Principal component analysis was performed (A) and a volcano plot was used to represent differentially expressed genes (DEGs in gray) (B). Red genes are Th1-associated DEGs, blue genes are Th2-associated DEGs. *n*=3-4. (C-E) Expression of Ly6C was analyzed by flow cytometry on blood monocytes (C; *n*=9-13), skeletal muscle (D; *n*=3-5) and white adipose tissue (WAT) resident macrophages (E; *n*=3-5). (F) Representative gating of the flow cytometry data presented in C-E. WT versus IL5-Tg: **P*<0.05, ****P*<0.001 [two-way ANOVA was performed followed by post-hoc testing (Šidak multiple comparison)]. Gaussian distribution was not assumed. Data are mean±s.e.m.

hyper-eosinophilia) drive the generation of a Th2 environment. To highlight a relationship between hyper-eosinophilia and macrophage polarization, we analyzed the expression of Ly6C on blood monocytes (MO) and tissue-resident macrophages from skeletal muscle and white adipose tissue (WAT). As expected, the expression of Ly6C on blood MO was severely affected, with Ly6C+ MOs representing 56% of the population in WT mice but only 12% in the IL5-Tg mice (P<0.001; Fig. 2C,F). In contrast, we did not observe significant changes in the Ly6C+ population in skeletal muscle (Fig. 2D,F). Strikingly, we instead observed an increase of the proportion of Ly6C+ macrophages in WAT (P<0.01; Fig. S2E,F). In aggregate, these data suggest that the number and function of eosinophils must be carefully balanced in order to contribute to a restorative Th2 response, and that changing their levels or altering their activation status can result in homeostatic changes that lead to failed regeneration. Moreover, we confirm here that hyper-eosinophilia is not necessarily linked to healthy Th2 inflammation in all tissues.

Muscle eosinophilia worsens tissue pathology

After observing the impact of hyper-eosinophilia on regeneration during acute injury, we sought to determine whether it also plays a role in a mouse model of chronic disease. A murine model of DMD (D2-*mdx*) was generated, wherein IL5 was also overexpressed (*mdx*:IL5-Tg). Strikingly, *mdx*:IL5-Tg mice exhibited decreased survival, with over 50% dying by 6 months of age, whereas the *mdx*:WT mice survived up to 12 months of age (Fig. 3A). Muscle mass and histopathology were assessed at 6/7 and 12 months of age. Overall, *mdx*:IL5-Tg mice displayed a reduction in body mass (P<0.01), with a decrease of 22% and 28% (P<0.05) at 6/7 and 12 months (Fig. 3B). Upon calculating muscle to body mass ratio (Table S1), we found no significant changes in TA weight ratio, likely due to the small sample size (n=3-6) (Fig. 3C). However, we observed decreases in gastrocnemius (GC) and quadriceps (Quad) weight ratios between *mdx*:WT and *mdx*:IL5-Tg mice (P<0.05 and P<0.001; Fig. 3D,E). The histopathology of *mdx*:IL5-Tg mice and their control littermates was assessed with laminin staining and

Development (2022) 149, dev200112. doi:10.1242/dev.200112

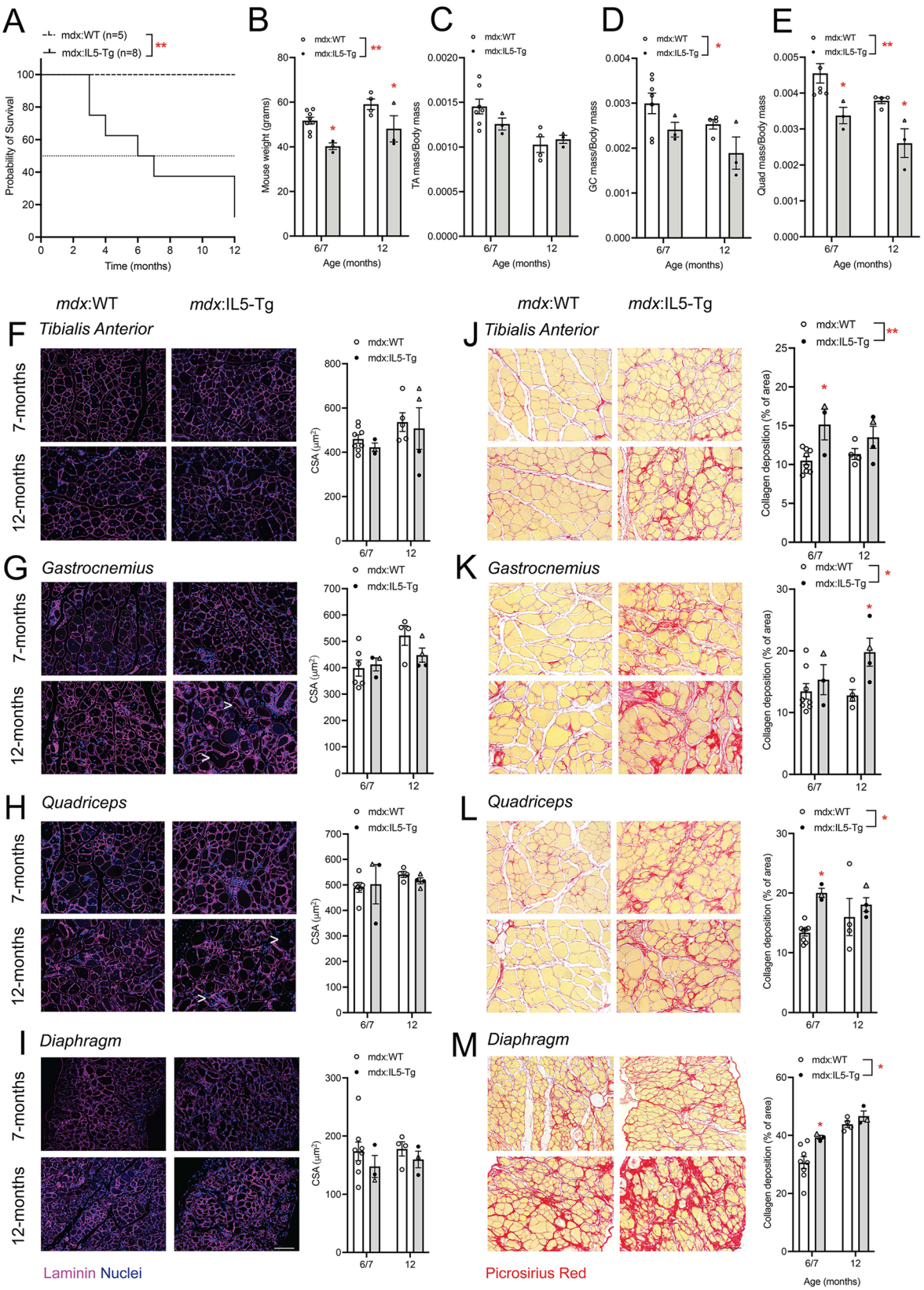

Fig. 3. Muscle histopathology worsens in *mdx*:IL5-Tg mice. (A) Survival curve of *mdx*:IL5-Tg mice and their control littermates. (B-E) At 6/7 and 12 months, mice were weighed (B) and tibialis anterior (TA) (C), gastrocnemius (GC) (D) and quadriceps (Quad) (E) muscle mass measured to calculate muscle mass/body mass ratio. (F-M) Cross-sectional area (CSA) of myofibers was measured with laminin staining (F-I) and collagen deposition was quantified by Picrosirius Red (PSR) staining (J-M). *n*=3-8. Δ in graph represent mice harvested when found dead. White arrowheads indicate hypertrophic myofibers. *mdx*:WT versus *mdx*:IL5-Tg: **P*<0.05, ***P*<0.01 [two-way ANOVA was performed followed by post-hoc testing (Šidak multiple comparison)]. Gaussian distribution was not assumed. Data are mean±s.e.m. Scale bar: 100 µm.

Development (2022) 149, dev200112. doi:10.1242/dev.200112

Picrosirius Red (PSR) to quantify myofiber size and fibrosis (Table S1). Interestingly, *mdx*:IL5-Tg mice did not exhibit any change in average myofiber size compared with *mdx*:WT in TA, GC, Quad and diaphragm muscles at 6/7 and 12 months, albeit no significant difference in size was found, likely due to low replicate numbers in the *mdx*:IL5-Tg cohort (Fig. 3F-I). However, we did notice a dramatic change in myofiber shape, with the emergence of hypertrophic myofibers in the GC and Quad of *mdx*:IL5-Tg mice at 12 months of age (Fig. 3G,H, white arrowheads). This could be a marker of myofiber branching, which is a known phenotype of DMD (Faber et al., 2014). This also indicates poor muscle repair, with few newly formed myofibers (small fibers). Through PSR staining, we noted that *mdx*:IL5-Tg mice exhibit an overall increase in fibrosis in the TA (P<0.01; Fig. 3J), that reached +44% (P<0.05) and +18.8% (P=0.08) at 6/7 and 12 months of age, respectively. Similarly, the GC displayed increased collagen deposition at 12 months (P<0.05; +54.8%; Fig. 3K), as well as the Quad (Fig. 3L) at 6/7 and 12 months of age. Finally, diaphragm muscles displayed more fibrosis overall (P<0.05; Fig. 3M) and we noted high variability in the fibrotic deposition of *mdx*:IL5-Tg diaphragms compared with *mdx*:WT mice, resulting in areas with very few muscle fibers, which is likely the cause of early death of *mdx*:IL5-tg mice (Fig. S3). Moreover, a possible role of eosinophilia in the development of cardiomyopathies has previously been described (Diny et al., 2017), although we did not observe any overt fibrotic scarring in the hearts of dead *mdx*:IL5-Tg mice (data not shown). In *mdx* muscles, where cycles of degeneration and repair occur, eosinophils have been shown to produce perforin, a substance that attacks muscle fibers through pore formation and causes necrosis, which we show to be increased in IL5-Tg eosinophils (Fig. 2) (Cai et al., 2000). In summary, although our results are limited due to a low number of mice, we found that *mdx*:IL5-Tg mice, compared with controls, clearly have a shortened lifespan and exhibit a worsening histopathology in muscle with age, suggesting that hyper-eosinophilia exacerbates the typical symptoms of DMD, including collagen deposition and, consequently, earlier death. Although Sek et al. (2019) described a moderate influence of hyper-eosinophilia on muscle histopathology, here we observed a dramatic effect on muscle fibrosis, which eventually led to death. One main difference is that here we have used the D2-*mdx* mice (D2.B10-Dmdmdx/J), unlike the previous authors who used the classic *mdx* (C57BL/10ScSn-Dmd mdx/J) mouse model. The D2-*mdx* mouse model is known to have a more robust phenotype closely mimicking human DMD (Fukada et al., 2010), which could explain the difference between studies. Also, Sek et al. focused exclusively on the early onset of the disease (3-5 weeks of age) corresponding to an acute inflammatory response, whereas we have focused more on the chronic phase of the disease.

Eosinophilia exacerbates DMD pathology

Due to the low number of *mdx*:IL5-Tg mice reaching 6/7 to 12 months of age, we used microdamage (microD) to exacerbate the chronic damage caused by DMD and to induce the formation of fibrotic scarring in the TA muscle of younger *mdx* mice (Desguerre et al., 2012). At 3 months of age, *mdx*:IL5-Tg mice did not display loss in body weight (Fig. S4A). However, the mass of the microD TA was remarkably decreased compared with the non-damaged TA (−15%, P<0.05), and even more so when compared with the *mdx*:WT-microD TA (−32%, P<0.001; Fig. S4B; Table S1). In control mice, we observed that the microD protocol resulted in a 34% decrease in myofiber CSA (Fig. S4C,D), as expected. We saw a 49% decrease (P<0.01) in non-damaged TA CSA in *mdx*:IL5-Tg mice compared with undamaged controls and, upon microD, we observed a further decrease of 57% (P<0.01) in the CSA between the two groups (Table S1). This defect in myofiber size was associated with a strong increase in collagen deposition and scarring, as shown with PSR staining (+93%, P<0.001; Fig. S4E, F; Table S1). This last experiment confirmed that hyper-eosinophilia participates in the pathologic progression of the muscle histopathology, specifically decreasing myofiber growth and increasing fibrosis deposition within the muscle. Taken together, our results and the results from Sek et al. (2019) support a model where eosinophils do not participate in the early onset of the disease, but continuous hyper-eosinophilia will eventually affect chronic muscle repair and accelerate the fibrotic deposition. Muscle eosinophilia has previously been associated with myositis; however, it does not appear to be always associated with poor outcomes (Selva-O'Callaghan et al., 2014), and although muscle eosinophilia has been investigated in autosomal-recessive limb girdle muscular dystrophies (LGMD2A/2C), to our knowledge it has not been fully investigated in DMD (Schröder et al., 2013). Based on the data provided here, assessment of eosinophils in human DMD is clearly warranted and simple peripheral blood eosinophil counts could be explored as a biomarker for the advanced stage of the disease and guide the appropriate choice of treatment.

MATERIALS AND METHODS

Mice

Mice were maintained in an enclosed and pathogen-free facility, housed in standard cages under 12 h light/dark cycles and fed *ad libitum* with a standard chow diet. All experimental procedures were approved by the University of British Columbia Animal Care Committee. IL5-Tg [Tg(Cd3d-Il5)NJ.1638Nal; Lee et al., 1997] and control littermate adult male mice (>8-weeks-old) were used for NTX injury. Acute muscle damage was induced by intramuscular injection of 0.15µg NTX snake venom (Latoxan), into the TA muscle. Then 0.5 mg of EdU was injected intraperitoneally the evening before harvesting (Click-IT plus EdU proliferation kit, Thermo Fisher Scientific). For co-culture experiments, TA and GC muscles of adult female WT and IL5-Tg littermates were damaged with NTX.

IL5-Tg male mice were bred for one generation with D2-*mdx* females (D2.B10-Dmdmdx/J, The Jackson Laboratory, #013141; Fukada et al., 2010). Only male littermates were used for experiments; micro-damage (microD) was performed as previously described (Desguerre et al., 2012) by injuring the TA muscle with 15 daily micro-needle pricks. TA muscles were harvested 1 week after the last day of injury.

Blood was collected from the saphenous vein: 1-2 drops of blood were collected in 1× PBS 2 mM EDTA and centrifuged at 300 ***g*** for 5 min at 4°C. Red blood cells were lysed using ACK lysis buffer (Gibco) and peripheral blood mononuclear cells (PBMCs) were stained with fluorophore-conjugated antibodies for detecting eosinophils as described below.

Histology

Mice were weighed, TA, GC, Quad and diaphragm muscles were harvested without fascia, weighed and fixed in 1% paraformaldehyde (PFA) overnight before being transferred to 70% ethanol. Muscles were embedded in paraffin and then sectioned at a thickness of 4 µm using a Leica microtome (RM 2255). Sections were stained with Hematoxylin and Eosin (H&E), PSR (Waxit) or laminin (Theret et al., 2021).

For immunostaining, damaged TAs were harvested, frozen in isopentane pre-cooled in liquid-nitrogen and stored at −80°C. We prepared 8 µm sections that were fixed with 4% PFA and saturated with blocking buffer (1× PSB, 3% goat serum, 0.3% Triton X-100). Primary antibodies (siglecF: Invitrogen, 14-1702-80, 1:200; laminin: Abcam, ab11575, 1:200) were incubated overnight at 4°C. Secondary antibodies (Invitrogen, A21247 and A11011; 1:1000) were incubated for 2 h at room temperature and DAPI (Invitrogen, D3571; 0.6 µM) was used to counterstain nuclei.

Development (2022) 149, dev200112. doi:10.1242/dev.200112

Imaging

Images were acquired using a Nikon Eclipse Ni equipped with a dual-use monochromatic and color imaging camera (Nikon Digital Sight DS-U3 for brightfield, Qimaging Retiga EXi for fluorescence), operated via NIS-Elements software. We used 10× and 20× objectives for stitching complete tissue images from tiles and for representative images in figures. Collagen deposition of the whole muscle section (PSR) was calculated using Adobe Illustrator CS6 and Fiji (ImageJ, version 2.0.0-rc/69/1.52n). CSA of the whole muscle section (laminin) was calculated using Fiji and Open-CSA macro (Desgeorges et al., 2019). Images were assembled using Adobe Illustrator CS6.

Flow cytometry analysis

Mice were anesthetized using avertin, followed by cardiac puncture, and perfused with 20 ml of 1× PBS 2 mM EDTA. Muscles were harvested without fascia, minced and digested for 1 h in 1.5 U/ml collagenase D (Millipore Sigma, 11 088 882 001), 2.4 U/ml Dispase II (Millipore Sigma, 04 942 078 001) and 10 mM $CaCl_2$ at 37°C. The cell suspension was diluted in FACS Buffer [1× PBS, 2% fetal bovine serum (FBS), 2 mM EDTA] and passed through a 40 µm filter. After a 20-min incubation in FACS buffer with 1:1000 Fc Receptor-blocking antibody (AbLab), cells were stained with antibodies listed in Table S2. For the proliferation assay, cells were stained for EdU incorporation as described in the manufacturer's manual (Click-iT Plus EdU kit; Thermo Fisher Scientific). Cell populations were acquired using LSRII (BD Biosciences) and Diva software. Flow data was then analyzed using FlowJoTM (BD Biosciences).

FAP sorting

Briefly, 3 days after NTX, muscles were harvested and digested as described above and stained for FAPs (antibodies in Table S2). FAPs (CD31−/CD45−/α7int− SCA1+ cells) were sorted using Astrios cell sorter (Beckman Coulter) and plated at 52,000 cells/cm^2 in six-well plates in 4.5 g/l glucose Dulbecco's modified eagle medium (DMEM; Invitrogen) supplemented with 1% sodium pyruvate, 10% FBS and 2.5 ng/ml bFGF (Invitrogen).

Single myofiber and FAP co-culture

FAPs and myofibers were co-cultured as previously described (Fiore et al., 2016). Briefly, 4 days after FAP sorting, single myofibers from WT extensor digitorum longus muscles were extracted as described by Brun et al. (2018) and placed in FBS-coated Bowden chambers (Falcon, 353102). Chambers containing 50-60 single myofibers were placed on top of previously sorted FAPs in 4.5 g/l glucose DMEM supplemented with 5% FBS and 0.5% chick embryo extract. After 47 h or 71 h of co-culture, myofibers were incubated for 1 h with 20 µM EdU before being harvested, fixed with 4% PFA and stained for Pax7/EdU/MyoD (48 h) or Pax7/Edu/myogenin (72 h), as previously described in Brun et al. (2018). Quantification was carried out using a Nikon Eclipse Ni equipped with a dual-use monochromatic Qimaging Retiga EXi camera and operated via NIS-Elements software. Representative images were taken using a 40× objective.

Eosinophil sorting and RNA extraction

Three days after NTX damage, mice were anesthetized using avertin, followed by cardiac puncture and perfusion with 20 ml of 1× PBS 2 mM EDTA. Muscles were carefully dissected and digested as described above. The cell suspension was stained using a panel of antibodies listed in Table S2, and eosinophils (CD45+ Ly6G−/NK1−/CD3− CD11b+ SiglecF+ cells) were directly collected into RNAzol using the Influx sorter (Becton Dickinson). RNA was extracted using the Direct-zol RNA Miniprep (Zymo Research).

Eosinophil RNA-seq bioinformatics analysis

Sample quality was assessed using the Agilent 2100 Bioanalyzer. RNA samples were prepared in accordance with the protocol for the TruSeq Stranded mRNA library kit (Illumina) on the Illumina Neoprep automated microfluidic library prep instrument. Paired-end sequencing was performed on the Illumina NextSeq 500 using the High Output 150 cycle Kit (Illumina). Illumina base call files were de-multiplexed using bcl2fastq2 (v 2.20) on BaseSpace. Adaptor sequences were trimmed and low-quality reads (<35 base pairs) were discarded. In addition, Bowtie was used to remove read pairs that aligned against abundant sequences. Demultiplexed read sequences were then aligned to the mm10 genome reference using STAR aligner. The number of aligned reads to each annotated gene was tallied with RnaReadCounter to generate read-count matrices for all samples, which were used as inputs for downstream analyses. Bowtie, STAR and RnaReadCounter are tools built under RNA-Seq Alignment (v 1.1.1). Downstream analyses of read-count data were performed in R (v 3.6.2). Genes with less than 2 counts per million (CPMs) in at least three samples were filtered out. Batch correction was applied using RUVSeq (v 1.20.0; Risso et al., 2014) where 3000 least-significant DEGs generated from a first-pass differential expression analysis were used as '*in-silico*' controls to estimate unwanted factors of variation. Batch-adjusted counts were normalized by upper-quartile normalization with EDASeq (v 2.20.0; Risso et al., 2011) before being subjected to PCA. Filtered counts were reprocessed and analyzed using DESeq2 (v 1.26.0 (Love et al., 2014)), incorporating two factors of unwanted variation (k=2) from the RUVg function in the design formula. Analyses in DESeq2 included count normalization and differential expression analysis. Volcano plot shown in Fig. 2B was generated using the EnhancedVolcano package (v 1.12.0; https://github.com/kevinblighe/EnhancedVolcano). All *P*-values were adjusted using the Benjamini-Hochberg correction.

Statistical analysis

Graphs were plotted and statistical tests performed using Prism 8 (GraphPad Software). Unpaired two-tailed Student's *t*-test or two-way ANOVA were performed, followed by post-hoc testing (Šidák multiple comparison). $P<0.05$ was considered statistically significant. Gaussian distribution was not assumed. Sample size for each experiment is indicated in the figure legends. Data represented in graphs are mean values with each individual replicate value plotted±standard error of the mean. Figures were assembled using Adobe Illustrator CS6.

Acknowledgements

The authors thank Justin Wong and Andrew Johnson from the UBC Flow Core, as well as Ryan Vander Werff, Tara Stach, Bernie Zhao and Dennis Okello from the BRC-Seq.

Competing interests

The authors declare no competing or financial interests.

Author contributions

Conceptualization: M.T., M.M., M.H., K.M., F.R.; Methodology: M.T., M.R.; Validation: M.T.; Formal analysis: M.T., L.R., J.H., L.W.T.; Investigation: M.T.; Data curation: M.T., L.R., M.R., F.F.L.; Writing - original draft: M.T., L.R.; Writing - review & editing: M.T., L.R., J.H., M.R., L.W.T., F.F.L., M.M., M.H., K.M., F.R.; Visualization: M.T.; Supervision: M.T., F.R.; Project administration: F.R.; Funding acquisition: M.T., F.R.

Funding

This work was supported by the Fondation pour la Recherche Médicale (FRM; 40248 to M.T.), the European Molecular Biology Organization (EMBO; ALTF 115-2016 to M.T.), by the Association Française contre les Myopathies (AFM; 22576 to M.T.), by Michael Smith Foundation for Health Research (MSFHR; 18351 to M.T.), by the Centre for Blood Research, University Of British Columbia (to L.R.) and by the Canadian Institutes of Health Research (CIHR-FDN-159908 to F.R. and CIHR-FRN-156235 to K.M.).

Data availability

RNA-seq datasets generated in the current study are available in the NCBI Gene Expression Omnibus under the accession number GSE189846.

Peer review history

The peer review history is available online at https://journals.biologists.com/dev/article-lookup/doi/10.1242/dev.200112.

References

Arnold, L., Henry, A., Poron, F., Baba-Amer, Y., Van Rooijen, N., Plonquet, A., Gherardi, R. K. and Chazaud, B. (2007). Inflammatory monocytes recruited after skeletal muscle injury switch into antiinflammatory macrophages to support myogenesis. *J. Exp. Med.* **204**, 1057-1069. doi:10.1084/jem.20070075

Bladen, C. L., Salgado, D., Monges, S., Foncuberta, M. E., Kekou, K., Kosma, K., Dawkins, H., Lamont, L., Roy, A. J., Chamova, T. et al. (2015). The TREAT-NMD DMD global database: analysis of more than 7,000 duchenne muscular dystrophy mutations. *Hum. Mutat.* **36**, 395-402. doi:10.1002/humu.22758

Bochner, B. S., Book, W., Busse, W. W., Butterfield, J., Furuta, G. T., Gleich, G. J., Klion, A. D., Lee, J. J., Leiferman, K. M., Minnicozzi, M. et al. (2012). Workshop report from the national institutes of health taskforce on the research needs of eosinophil-associated diseases (TREAD). *J. Allergy Clin. Immunol.* **130**, 587-596. doi:10.1016/j.jaci.2012.07.024

Brigger, D., Riether, C., Van Brummelen, R., Mosher, K. I., Shiu, A., Ding, Z., Zbären, N., Gasser, P., Guntern, P., Yousef, H. et al. (2020). Eosinophils regulate adipose tissue inflammation and sustain physical and immunological fitness in old age. *Nat. Metab.* **2**, 688-702. doi:10.1038/s42255-020-0228-3

Brun, C. E., Wang, Y. X. and Rudnicki, M. A. (2018). Single EDL myofiber isolation for analyses of quiescent and activated muscle stem cells. Methods Mol. Biol. **1686**, 149-159. doi:10.1007/978-1-4939-7371-2_11

Cai, B., Spencer, M. J., Nakamura, G., Tseng-Ong, L. and Tidball, J. G. (2000). Eosinophilia of dystrophin-deficient muscle is promoted by perforin-mediated cytotoxicity by T cell effectors. *Am. J. Pathol.* **156**, 1789-1796. doi:10.1016/S0002-9440(10)65050-X

Chazaud, B. (2020). Inflammation and skeletal muscle regeneration: leave it to the macrophages!. *Trends Immunol.* **41**, 481-492. doi:10.1016/j.it.2020.04.006

Dadgar, S., Wang, Z., Johnston, H., Kesari, A., Nagaraju, K., Chen, Y.-W., Hill, D. A., Partridge, T. A., Giri, M., Freishtat, R. J. et al. (2014). Asynchronous remodeling is a driver of failed regeneration in Duchenne muscular dystrophy. *J. Cell Biol.* **207**, 139-158. doi:10.1083/jcb.201402079

Desgeorges, T., Liot, S., Lyon, S., Bouvière, J., Kemmel, A., Trignol, A., Rousseau, D., Chapuis, B., Gondin, J., Mounier, R. et al. (2019). Open-CSAM, a new tool for semi-automated analysis of myofiber cross-sectional area in regenerating adult skeletal muscle. *Skelet. Muscle* **9**, 2. doi:10.1186/s13395-018-0186-6

Desguerre, I., Arnold, L., Vignaud, A., Cuvellier, S., Yacoub-Youssef, H., Gherardi, R. K., Chelly, J., Chretien, F., Mounier, R., Ferry, A. et al. (2012). A new model of experimental fibrosis in hindlimb skeletal muscle of adult mdx mouse mimicking muscular dystrophy. *Muscle Nerve* **45**, 803-814. doi:10.1002/mus.23341

Diny, N. L., Baldeviano, G. C., Talor, M. V., Barin, J. G., Ong, S. F., Bedja, D., Hays, A. G., Gilotra, N. A., Coppens, I., Rose, N. R. et al. (2017). Eosinophil-derived IL-4 drives progression of myocarditis to inflammatory dilated cardiomyopathy. *J. Exp. Med.* **214**, 943-957. doi:10.1084/jem.20161702

Dolitzky, A., Shapira, G., Grisaru-Tal, S., Hazut, I., Avlas, S., Gordon, Y., Itan, M., Shomron, N. and Munitz, A. (2021). Transcriptional profiling of mouse eosinophils identifies distinct gene signatures following cellular activation. *Front. Immunol.* **12**, 1-15. doi:10.3389/fimmu.2021.802839

Dougan, M., Dranoff, G. and Dougan, S. K. (2019). GM-CSF, IL-3, and IL-5 family of cytokines: regulators of inflammation. *Immunity* **50**, 796-811. doi:10.1016/j.immuni.2019.03.022

Drake, M. G., Bivins-Smith, E. R., Proskocil, B. J., Nie, Z., Scott, G. D., Lee, J. J., Lee, N. A., Fryer, A. D. and Jacoby, D. B. (2016). Human and mouse eosinophils have antiviral activity against parainfluenza virus. *Am. J. Respir. Cell Mol. Biol.* **55**, 387-394. doi:10.1165/rcmb.2015-0405OC

Dumont, N. A., Wang, Y. X., Von Maltzahn, J., Pasut, A., Bentzinger, C. F., Brun, C. E. and Rudnicki, M. A. (2015). Dystrophin expression in muscle stem cells regulates their polarity and asymmetric division. *Nat. Med.* **21**, 1455-1463. doi:10.1038/nm.3990

Faber, R. M., Hall, J. K., Chamberlain, J. S. and Banks, G. B. (2014). Myofiber branching rather than myofiber hyperplasia contributes to muscle hypertrophy in mdx mice. *Skelet. Muscle* **4**, 10. doi:10.1186/2044-5040-4-10

Fiore, D., Judson, R. N., Low, M., Lee, S., Zhang, E., Hopkins, C., Xu, P., Lenzi, A., Rossi, F. M. and Lemos, D. R. (2016). Pharmacological blockage of fibro/adipogenic progenitor expansion and suppression of regenerative fibrogenesis is associated with impaired skeletal muscle regeneration. *Stem Cell Res.* **17**, 161-169. doi:10.1016/j.scr.2016.06.007

Fukada, S.-I., Morikawa, D., Yamamoto, Y., Yoshida, T., Sumie, N., Yamaguchi, M., Ito, T., Miyagoe-Suzuki, Y., Takeda, S., Tsujikawa, K. et al. (2010). Genetic background affects properties of satellite cells and mdx phenotypes. *Am. J. Pathol.* **176**, 2414-2424. doi:10.2353/ajpath.2010.090887

Giordani, L., Parisi, A. and Le Grand, F. (2018). Satellite cell self-renewal. *Curr. Top. Dev. Biol.* **126**, 177-203. doi:10.1016/bs.ctdb.2017.08.001

Girardi, F., Taleb, A., Ebrahimi, M., Datye, A., Gamage, D. G., Peccate, C., Giordani, L., Millay, D. P., Gilbert, P. M., Cadot, B. et al. (2021). TGFβ signaling curbs cell fusion and muscle regeneration. *Nat. Commun.* **12**, 750. doi:10.1038/s41467-020-20289-8

Heredia, J. E., Mukundan, L., Chen, F. M., Mueller, A. A., Deo, R. C., Locksley, R. M., Rando, T. A. and Chawla, A. (2013). Type 2 innate signals stimulate fibro/adipogenic progenitors to facilitate muscle regeneration. *Cell* **153**, 376-388. doi:10.1016/j.cell.2013.02.053

Joe, A. W. B., Yi, L., Natarajan, A., Le Grand, F., So, L., Wang, J., Rudnicki, M. A. and Rossi, F. M. V. (2010). Muscle injury activates resident fibro/adipogenic progenitors that facilitate myogenesis. *Nat. Cell Biol.* **12**, 153-163. doi:10.1038/ncb2015

Juban, G. (2021). Transcriptional control of macrophage inflammatory shift during skeletal muscle regeneration. *Semin. Cell Dev. Biol.* **119**, 82-88. doi:10.1016/j.semcdb.2021.06.011

Juban, G., Saclier, M., Yacoub-Youssef, H., Kernou, A., Arnold, L., Boisson, C., Ben Larbi, S., Magnan, M., Cuvellier, S., Théret, M. et al. (2018). AMPK activation regulates LTBP4-dependent TGF-β1 secretion by pro-inflammatory macrophages and controls fibrosis in Duchenne muscular dystrophy. *Cell Rep.* **25**, 2163-2176.e6. doi:10.1016/j.celrep.2018.10.077

Kastenschmidt, J. M., Coulis, G., Farahat, P. K., Pham, P., Rios, R., Cristal, T. T., Mannaa, A. H., Ayer, R. E., Yahia, R., Deshpande, A. A. et al. (2021). A stromal progenitor and ILC2 niche promotes muscle eosinophilia and fibrosis-associated gene expression. *Cell Rep.* **35**, 108997. doi:10.1016/j.celrep.2021.108997

Lee, J. J., Mcgarry, M. P., Farmer, S. C., Denzler, K. L., Larson, K. A., Carrigan, P. E., Brenneise, I. E., Horton, M. A., Haczku, A., Gelfand, E. W. et al. (1997). Interleukin-5 expression in the lung epithelium of transgenic mice leads to pulmonary changes pathognomonic of asthma. *J. Exp. Med.* **185**, 2143-2156. doi:10.1084/jem.185.12.2143

Lemos, D. R., Babaeijandaghi, F., Low, M., Chang, C.-K., Lee, S. T., Fiore, D., Zhang, R.-H., Natarajan, A., Nedospasov, S. A. and Rossi, F. M. V. (2015). Nilotinib reduces muscle fibrosis in chronic muscle injury by promoting TNF-mediated apoptosis of fibro/adipogenic progenitors. *Nat. Med.* **21**, 786-794. doi:10.1038/nm.3869

Lepper, C., Partridge, T. A. and Fan, C.-M. (2011). An absolute requirement for Pax7-positive satellite cells in acute injury-induced skeletal muscle regeneration. *Development* **138**, 3639-3646. doi:10.1242/dev.067595

Love, M. I., Huber, W. and Anders, S. (2014). Moderated estimation of fold change and dispersion for RNA-seq data with DESeq2. *Genome Biol.* **15**, 550. doi:10.1186/s13059-014-0550-8

Muller, J., Vayssiere, N., Royuela, M., Leger, M. E., Muller, A., Bacou, F., Pons, F., Hugon, G. and Mornet, D. (2001). Comparative evolution of muscular dystrophy in diaphragm, gastrocnemius and masseter muscles from old male mdx mice. *J. Muscle Res. Cell Motil.* **22**, 133-139. doi:10.1023/A:1010305801236

Murphy, M. M., Lawson, J. A., Mathew, S. J., Hutcheson, D. A. and Kardon, G. (2011). Satellite cells, connective tissue fibroblasts and their interactions are crucial for muscle regeneration. *Development* **138**, 3625-3637. doi:10.1242/dev.064162

Oprescu, S. N., Yue, F., Qiu, J., Brito, L. F. and Kuang, S. (2020). Temporal dynamics and heterogeneity of cell populations during skeletal muscle regeneration. *iScience* **23**, 100993. doi:10.1016/j.isci.2020.100993

Otis, J. S., Niccoli, S., Hawdon, N., Sarvas, J. L., Frye, M. A., Chicco, A. J. and Lees, S. J. (2014). Pro-inflammatory mediation of myoblast proliferation. *PLoS ONE* **9**, e92363. doi:10.1371/journal.pone.0092363

Pastoret, C. and Sebille, A. (1995). mdx mice show progressive weakness and muscle deterioration with age. *J. Neurol. Sci.* **129**, 97-105. doi:10.1016/0022-510X(94)00276-T

Rana, B. M. J., Jou, E., Barlow, J. L., Rodriguez-Rodriguez, N., Walker, J. A., Knox, C., Jolin, H. E., Hardman, C. S., Sivasubramaniam, M., Szeto, A. et al. (2019). A stromal cell niche sustains ILC2-mediated type-2 conditioning in adipose tissue. *J. Exp. Med.* **216**, 1999-2009. doi:10.1084/jem.20190689

Ratnayake, D., Nguyen, P. D., Rossello, F. J., Wimmer, V. C., Tan, J. L., Galvis, L. A., Julier, Z., Wood, A. J., Boudier, T., Isiaku, A. I. et al. (2021). Macrophages provide a transient muscle stem cell niche via NAMPT secretion. *Nature* **591**, 281-287. doi:10.1038/s41586-021-03199-7

Risso, D., Schwartz, K., Sherlock, G. and Dudoit, S. (2011). GC-content normalization for RNA-seq data. *BMC Bioinformatics* **12**, 480. doi:10.1186/1471-2105-12-480

Risso, D., Ngai, J., Speed, T. P. and Dudoit, S. (2014). Normalization of RNA-seq data using factor analysis of control genes or samples. *Nat. Biotechnol.* **32**, 896-902. doi:10.1038/nbt.2931

Rodrigo-Muñoz, J. M., Gil-Martínez, M., Sastre, B. and Del Pozo, V. (2021). Emerging evidence for pleiotropism of Eosinophils. *Int. J. Mol. Sci.* **22**, 7075. doi:10.3390/ijms22137075

Rothenberg, M. E. and Hogan, S. P. (2006). The eosinophil. *Annu. Rev. Immunol.* **24**, 147-174. doi:10.1146/annurev.immunol.24.021605.090720

Sacco, A., Doyonnas, R., Kraft, P., Vitorovic, S. and Blau, H. M. (2008). Self-renewal and expansion of single transplanted muscle stem cells. *Nature* **456**, 502-506. doi:10.1038/nature07384

Saclier, M., Yacoub-Youssef, H., Mackey, A. L., Arnold, L., Ardjoune, H., Magnan, M., Sailhan, F., Chelly, J., Pavlath, G. K., Mounier, R. et al. (2013). Differentially activated macrophages orchestrate myogenic precursor cell fate during human skeletal muscle regeneration. *Stem Cells* **31**, 384-396. doi:10.1002/stem.1288

Sambasivan, R., Yao, R., Kissenpfennig, A., Van Wittenberghe, L., Paldi, A., Gayraud-Morel, B., Guenou, H., Malissen, B., Tajbakhsh, S. and Galy, A. (2011). Pax7-expressing satellite cells are indispensable for adult skeletal muscle regeneration. *Development* **138**, 3647-3656. doi:10.1242/dev.067587

Schröder, T., Fuchss, J., Schneider, I., Stoltenburg-Didinger, G. and Hanisch, F. (2013). Eosinophils in hereditary and inflammatory myopathies. *Acta Myol.* **32**, 148-153.

Sek, A. C., Moore, I. N., Smelkinson, M. G., Pak, K., Minai, M., Smith, R., Ma, M., Percopo, C. M. and Rosenberg, H. F. (2019). Eosinophils do not drive acute muscle pathology in the mdx mouse model of Duchenne muscular dystrophy. *J. Immunol.* **203**, 476-484. doi:10.4049/jimmunol.1900307

Selva-O'callaghan, A., Trallero-Araguás, E. and Grau, J. M. (2014). Eosinophilic myositis: an updated review. *Autoimmun Rev.* **13**, 375-378. doi:10.1016/j.autrev.2014.01.018

Takemura, N., Kurashima, Y., Mori, Y., Okada, K., Ogino, T., Osawa, H., Matsuno, H., Aayam, L., Kaneto, S., Park, E. J. et al. (2018). Eosinophil depletion suppresses radiation-induced small intestinal fibrosis. *Sci. Transl. Med.* **10**, eaan0333. doi:10.1126/scitranslmed.aan0333

Theret, M., Low, M., Rempel, L., Li, F. F., Tung, L. W., Contreras, O., Chang, C.-K., Wu, A., Soliman, H. and Rossi, F. M. V. (2021). In vitro assessment of anti-fibrotic drug activity does not predict in vivo efficacy in murine models of Duchenne muscular dystrophy. *Life Sci.* **279**, 119482. doi:10.1016/j.lfs.2021.119482

Tidball, J. G., Albrecht, D. E., Lokensgard, B. E. and Spencer, M. J. (1995). Apoptosis precedes necrosis of dystrophin-deficient muscle. *J. Cell Sci.* **108**, 2197-2204. doi:10.1242/jcs.108.6.2197

Uezumi, A., Fukada, S.-I., Yamamoto, N., Takeda, S. and Tsuchida, K. (2010). Mesenchymal progenitors distinct from satellite cells contribute to ectopic fat cell formation in skeletal muscle. *Nat. Cell Biol.* **12**, 143-152. doi:10.1038/ncb2014

Uezumi, A., Ito, T., Morikawa, D., Shimizu, N., Yoneda, T., Segawa, M., Yamaguchi, M., Ogawa, R., Matev, M. M., Miyagoe-Suzuki, Y. et al. (2011). Fibrosis and adipogenesis originate from a common mesenchymal progenitor in skeletal muscle. *J. Cell Sci.* **124**, 3654-3664. doi:10.1242/jcs.086629

Varga, T., Mounier, R., Patsalos, A., Gogolák, P., Peloquin, M., Horvath, A., Pap, A., Daniel, B., Nagy, G., Pintye, E. et al. (2016). Macrophage PPARγ, a lipid activated transcription factor controls the growth factor GDF3 and skeletal muscle regeneration. *Immunity* **45**, 1038-1051. doi:10.1016/j.immuni.2016.10.016

Wehling-Henricks, M. (2004). Prednisolone decreases cellular adhesion molecules required for inflammatory cell infiltration in dystrophin-deficient skeletal muscle. *Neuromuscul. Disord.* **14**, 483-490. doi:10.1016/j.nmd.2004.04.008

Wehling-Henricks, M., Sokolow, S., Lee, J. J., Myung, K. H., Villalta, S. A. and Tidball, J. G. (2008). Major basic protein-1 promotes fibrosis of dystrophic muscle and attenuates the cellular immune response in muscular dystrophy. *Hum. Mol. Genet.* **17**, 2280-2292. doi:10.1093/hmg/ddn129

Figure S1

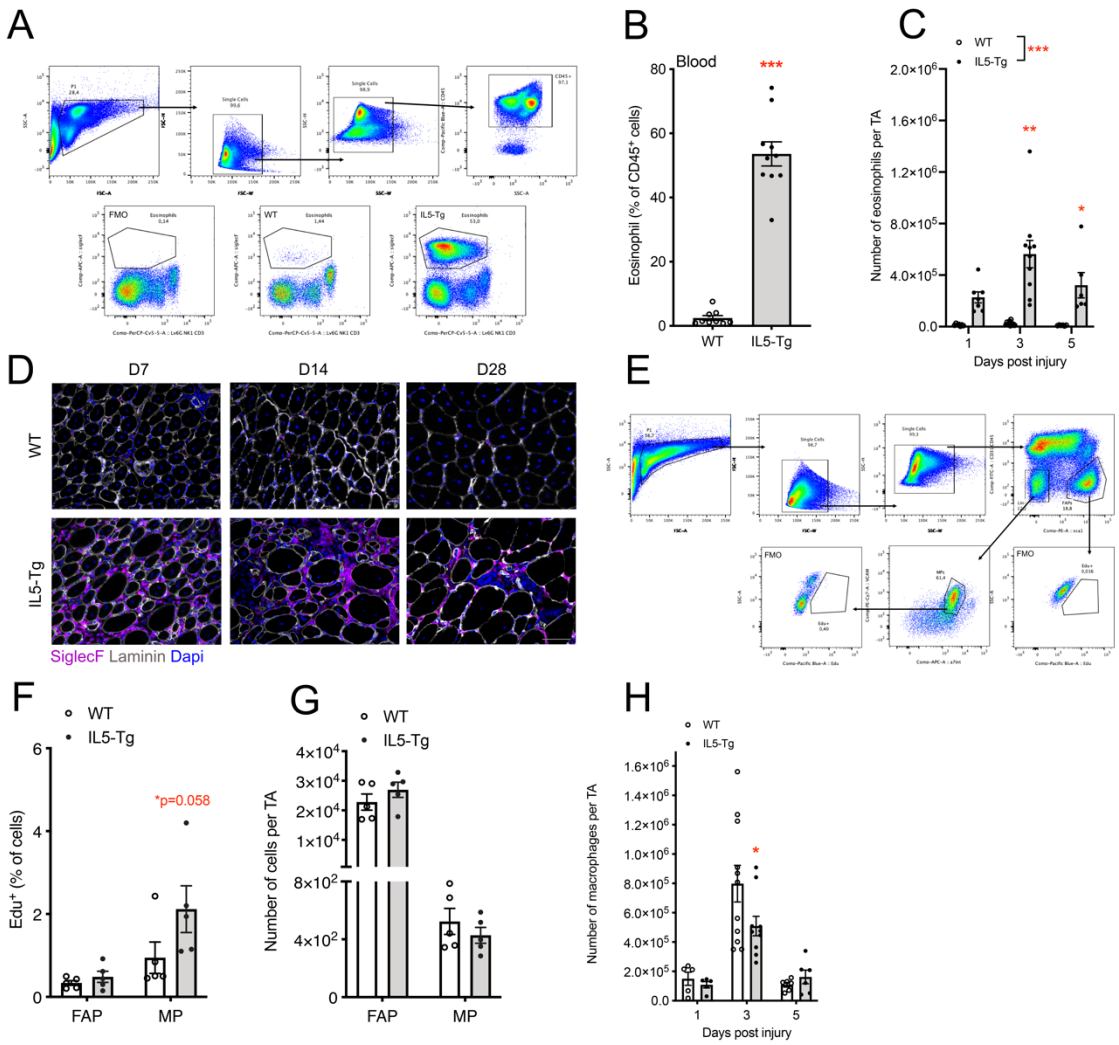

Fig. S1. Flow cytometry analysis of eosinophils, fibro-adipogenic, and myogenic progenitors. **(A-B)** Blood of IL5-Tg and littermate control mice was harvested and eosinophil content was analyzed by flow cytometry. n=9-10 (**C**) The same gating strategy was used to quantify eosinophil content in muscle after notexin (NTX) damage. n=5-10. (**D**) Eosinophil infiltration was validated by immunostaining against SiglecF. (**E-F**) One day after injury, activation of fibro-adipogenic progenitors (FAP) and myogenic progenitors (MP) was assessed with EdU incorporation and (**G**) their total number per TA was quantified. n=5

Figure S2

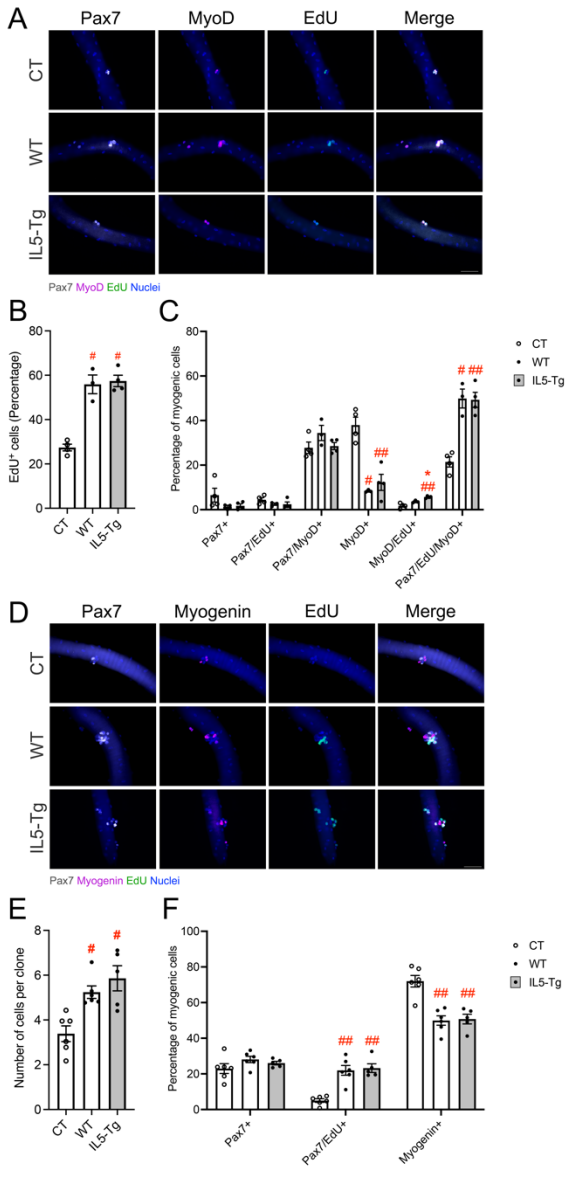

Fig. S2. Trophic effect of WT and IL5-Tg FAPs on satellite cell fate ex vivo.

WT single myofibers were cultured alone (CT), with WT or with IL5-Tg FAPs for 48h and 72h. (**A**) At 48h, myofibers were stained for Pax7 (White), EdU (Green), MyoD (Magenta) and DAPI (Blue). (**B**) Percentage of EdU+ myogenic cells was calculated and (**C**) satellite cell fate was analyzed by the expression of Pax7, MyoD, and EdU. n=3-4 (**D**) At 72h, myofibers were stained for Pax7 (White), EdU (Green), Myogenin (Magenta) and DAPI (Blue). (**E**) The number of cells per clone was calculated and (**F**) satellite cell fate was analyzed by the expression of Pax7, EdU, and Myogenin. n=5-6

CT versus WT or IL5-Tg: # $p<0.05$; ## $p<0.01$

WT versus IL5-Tg: * $p<0.05$

Scale bar: 100 µm

Figure S3

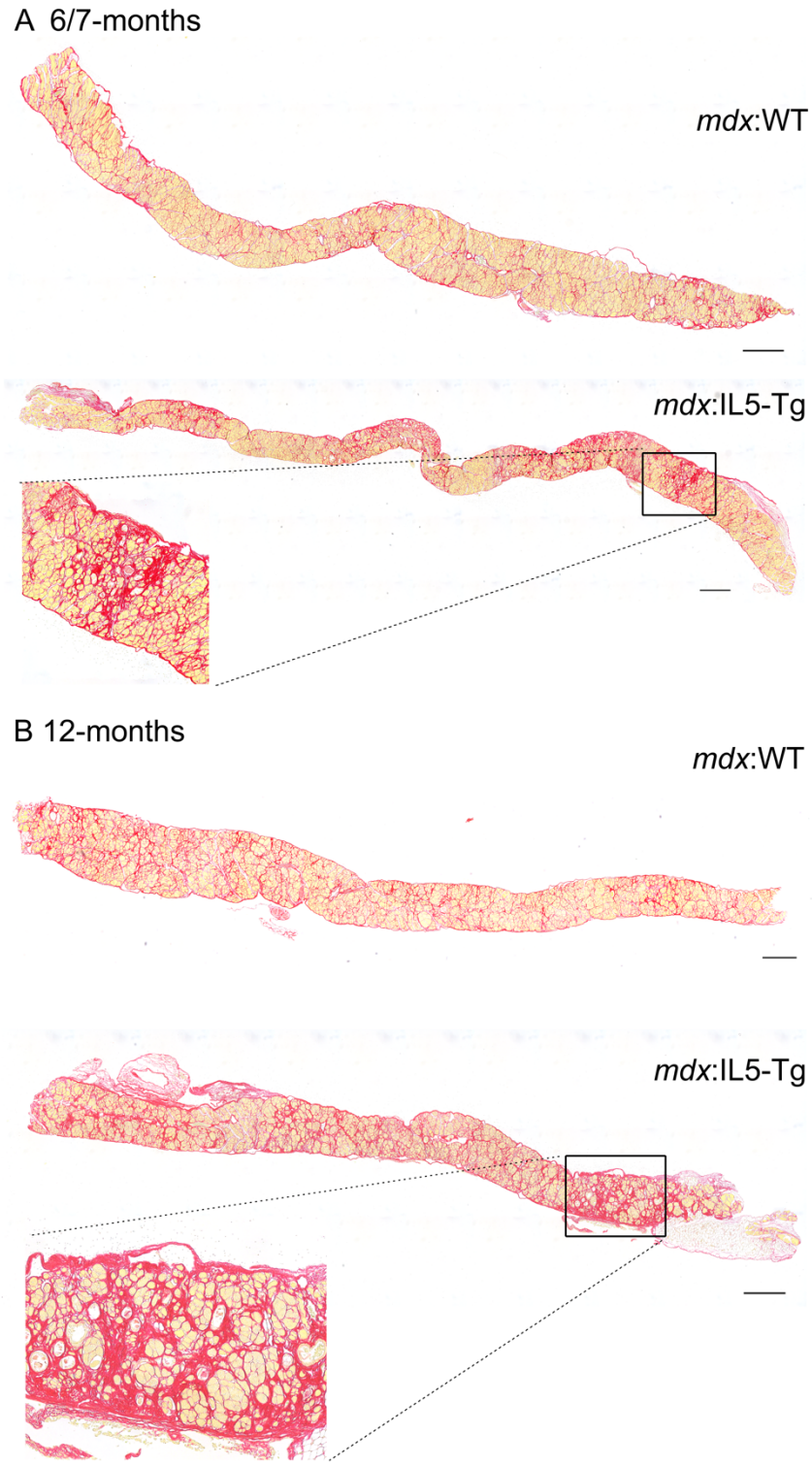

Fig. S3. Histopathology of mdx-IL5-Tg diaphragm

Picrosirius Red (PSR) colouration of *mdx*-WT and *mdx*-IL5-Tg diaphragm at (**A**) 7 months and (**B**) 12 months of age. Arrow highlights areas with elevated fibrotic deposition

Scale bar = 500 μm

Figure S4

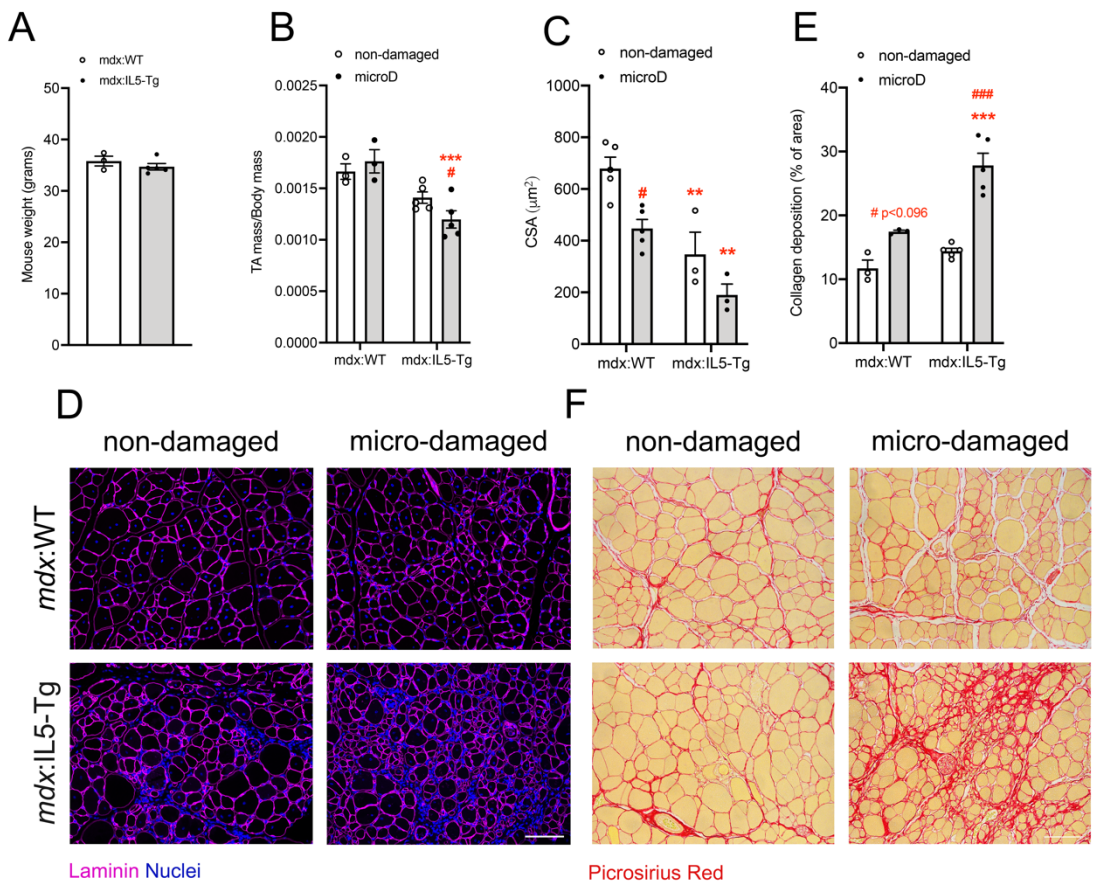

Fig. S4. Fibrosis deposition is accelerated in mdx:IL5-Tg mice.

Right tibialis anterior (TA) muscle of *mdx*:IL5-Tg mice and their control littermates were micro-damaged (microD) from 8 to 10 weeks of age. One week later, (**A-B**) mice and TAs were weighed and general histology was assessed. (**C**) Cross-sectional area (CSA) of myofibers was measured with (**D**) laminin staining and (**E**) collagen deposition was quantified by (**F**) picrosirius red (PSR) colouration. n=3-5

Non-damaged versus microD: # p<0.05; ### p<0.001

mdx:WT versus *mdx*:IL5-Tg: ** p<0.01; *** p<0.001

Scale bar: 100 μm

Table S1. Summary of results for mdx:IL5-Tg

Age	Mouse weight (g)	Muscle/body weight ratio (a.u.)	CSA (μm²)	Collagen (%)
3 months	35.8±1.3 vs 34.7±1.3 -3.1%	ND: 0.00166 vs 0.00141; -15.2% microD: 0.00176 vs 0.00120; -32.0%	ND: 679±88.4 vs 347.3±120.8; -48.8 MicroD: 447.2±66.7 vs 190.2±59.3; -57%	ND: 11.7±1.9 vs 14.4±0.9; +22.9% MicroD: 17.5±0.3 vs 27.8±3.8; +59.3%
6/7 months	51.7±4.1 vs 40.3±2.1 -22%	TA: 0.00143 vs 0.00126; -11.6% GC: 0.00305 vs 0.00241; -21.2% Quad: 0.00453 vs 0.00337; -25.6%	TA: 459±55 vs 422±27; -8.1% GC: 408±67 vs 412±34; +1.4% Quad: 482±45 vs 502±109; +4.3% Dia: 173±42 vs 147±27; -15%	TA: 10.5±3.5 vs 15.1±2.8; +44% GC: 13.4±5.2 vs 15.3±3.4; +14% Quad: 13.3±4.4 vs 20.0±1.1; +50.0% Dia: 30.6±10.9 vs 39.3±1.0 +28.5.0%
12 months	59±4.1 vs 42.2±0.8 -28%	TA: 0.00103 vs 0.00108; +5.6% GC: 0.00253 vs 0.00189; -25.2% Quad: 0.00379 vs 0.00260; -31.2%	TA: 498±41 vs 507±132; +1.8% GC: 522±64 vs 448±46; -14.2% Quad: 541±20 vs 516±20; -4.6% Dia: 177±21 vs 160±20; -10.2%	TA: 11.3±1.2 vs 13.5±2.5; +18.8% GC: 12.8±1.6 vs 19.8±3.9; +54.8% Quad: 16.0±5.4 vs 18.1±2.0; +13.0% Dia: 43.8±1.9 vs 46.6±2.9; +6.4%

Values presented are WT vs IL5-Tg; mean ± Standard Deviation (SD)

3-months old: *mdx*:WT n=3-5; *mdx*:IL5-Tg n=3-5
6/7-months old: *mdx*:WT n=8; *mdx*:IL5-Tg n=3
12-months old: *mdx*:WT n=4; *mdx*:IL5-Tg n=4 (Dia n=3)
TA: Tibialis Anterior
GC: Gastrocnemius
Quad: Quadriceps
Dia: Diaphragm
microD: microdamaged TA
ND: non-damaged TA

Table S2. Antibody list

Antibody	Clone	Dilution	Company/Catalogue
Anti-mouse Ly-6G (Gr-1)	1A8	1:200	BD #560602
anti-mouse NK1.1	PK136	1:200	Biolegend #108728
anti-mouse CD3e	145-2C11	1:400	Biolegend #100328
Anti-mouse CD45 (Pan)	30-F11	1:500	Biolegend #103154
Anti-mouse CD45 (Pan)	I3/2	1:400	AbLab #62-0047-01
Anti-mouse/human CD11b	M1/70	1:500	BD #9057925
Anti-mouse CD11c	N418	1:400	AbLab #48-0051-01
Anti-mouse Ly-6C	HK1.4	1:800	Biolegend #128018
Anti-mouse siglecF (CD170)	E50-2440	1:500	Biolegend #155508
Anti-mouse CD31	390	1:500	Ebioscience #11-0311-85
Anti-mouse SCA-1	D7	1:1000	Ebioscience #11-5981-81
Anti-mouse A7integrin	R2F2	1:3000	Ablab #67-0010-05
Anti-mouse VCAM	429 (MVCAM.A)	1:2000	Biolegend #105720

Table S3. Differentially expressed genes

Click here to download Table S3